

# STABILITY ANALYSIS OF 1 DOF HAPTIC INTERFACE: TIME DELAY AND VIBRATION MODES EFFECTS

Q. V. Dang<sup>(a)</sup>, A. Dequidt<sup>(b)</sup>, L. Vermeiren<sup>(c)</sup>, M. Dambrine<sup>(d)</sup>

<sup>(a,b,c,d)</sup> Univ Lille Nord de France, F-59000 Lille, France

<sup>(a,b,c,d)</sup> UVHC, LAMIH, F-59313 Valenciennes, France

<sup>(a,b,c,d)</sup> CNRS, UMR 8530, F-59313 Valenciennes, France

<sup>(a)</sup>[dqviet2212@gmail.com](mailto:dqviet2212@gmail.com), <sup>(b)</sup>[antoine.dequidt@univ-valenciennes.fr](mailto:antoine.dequidt@univ-valenciennes.fr),

<sup>(c)</sup>[laurent.vermeiren@univ-valenciennes.fr](mailto:laurent.vermeiren@univ-valenciennes.fr), <sup>(d)</sup>[michel.dambrine@univ-valenciennes.fr](mailto:michel.dambrine@univ-valenciennes.fr)

## ABSTRACT

Stability analysis continues to be a major challenge in the haptic field. This paper addresses the issue of stability for haptic interfaces in contact with a virtual wall. The feedback contact force is calculated from the impedance-based virtual environment model including a linear stiffness and a damping. A mechanical model includes two vibration modes used to characterize the overall device dynamics. Their effects on the stability and those of the time delay are examined. The stability boundary is derived from a sampled data model of the haptic interface by the gain margin method.

Keywords: Haptic device, Stability region, Time delay, Vibration mode

## 1. INTRODUCTION

Haptic system includes the human operator and the haptic interface, c.f. Fig.1. Haptic interface is the robotic system that allows human operator to manipulate objects in a Virtual Environment (VE) by a haptic device with the sense of touch and the kinesthetic perception.

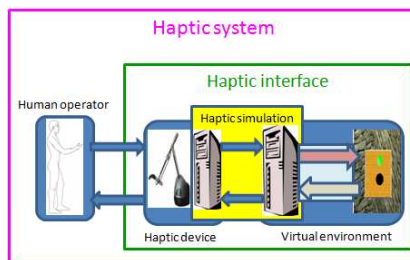


Figure 1: Parts of a haptic system

However, unlike robot manipulators, the haptic interfaces should have both high force rendering and maximum dynamic transparency (low inertia, low friction, etc.). Therefore, the stability of a haptic interface is a key issue. Any unstable behavior arising during the dynamic interaction can damage the haptic device or injure the human operator.

Nowadays, there are two main approaches to study the stability of a haptic system. In the first approach

(Gil and al. 2004; Diolaiti and al. 2006; Hulin and al. 2006; Hulin and al. 2008), the haptic system is described by a sampled-data model; the VE is seen as a virtual impedance characterized by a linear spring and a damper. The stability region is represented by the stability boundaries in the stiffness-damping plan of the virtual impedance. The influence of parameters such as physical damping and time delay on the stability boundaries is evaluated through the transfer function. The human hand impedance can be included in the model to study the human dynamic effects. In the second approach, the two-port network theory is applied to separate the virtual environment and the human operator into two independent parts (Colgate and Brown 1994; Colgate and Schenkel 1997; Adams and Hannaford 1998; Adams and al. 1998; Adams and Hannaford 1999; Adams and Hannaford 2002). Then, the virtual coupling is used and the stability is ensured through the passivity or unconditional stability criteria.

There are a lot of works concerning the interaction of the human operator, the haptic device and the virtual environment. However, there still remain many challenges such as expanding the boundary of stability region, modeling the human operator, designing the control law, etc. In previous studies, the haptic device was modeled as a mechanical system including a mass and a physical damper. The existence of vibration modes in the haptic device has been studied recently (Díaz and Gil 2008; Díaz and Gil 2008), but these works have not fully explained the influence of the vibration mode parameters.

The contribution of this paper consists in analyzing the mechanical frequency effects of the haptic device's vibration modes and the time delay influence on the interface stability based on the first approach. The results are carried out on the physical parameters of the PHANTOM<sup>®</sup> haptic device.

## 2. HAPTIC DEVICE MODELING

In previous studies, a rigid model of haptic device is used to analyze the stability. In this paper, the elastic deformations are considered in the mechanical transmission between motor and human hand. Consequently, the resulting vibration modes can modify

the stability boundaries. That's why a more complete model of haptic device with two most significant vibration modes is shown in fig.2. These vibration modes result from 1) the elastic joint between the motor (position  $X_1$ ) and the link shaft (position  $X_2$ ) and 2) the flexible link between the shaft and the tip (position  $X_3$ ). The motor applies a force  $F_1$  and the human hand laid on the link tip applies a force  $F_h$ . With the mechanical parameters pointed out on fig.2, the linear model can be derived in Laplace domain as:

$$(\mathbf{M}s^2 + \mathbf{B}s + \mathbf{K})\mathbf{X}(s) = \mathbf{F}(s) \quad (1)$$

with the position and force vector and the mass, damping and stiffness matrices, respectively:

$$\mathbf{X}(s) = [X_1(s) X_2(s) X_3(s)]^T \quad (2)$$

$$\mathbf{F}(s) = [F_1(s) F_h(s)]^T \quad (3)$$

$$\mathbf{M}(s) = \text{diag}(m_1, m_2, m_3) \quad (4)$$

$$\mathbf{B}(s) = \begin{bmatrix} b_{c1} + b_1 & -b_{c1} & 0 \\ -b_{c1} & b_{c1} + b_{c2} + b_2 & -b_{c2} \\ 0 & -b_{c2} & b_{c2} + b_3 \end{bmatrix} \quad (5)$$

$$\mathbf{K}(s) = \begin{bmatrix} k_{c1} & -k_{c1} & 0 \\ -k_{c1} & k_{c1} + k_{c2} & -k_{c2} \\ 0 & -k_{c2} & k_{c2} \end{bmatrix} \quad (6)$$

The relationship between output positions and input forces is presented on the form of a transfer function matrix:

$$\mathbf{X}(s) = \mathbf{G}(s)\mathbf{F}(s) \quad (7)$$

with:

$$\mathbf{G}(s) = \begin{bmatrix} G_{11}(s) & G_{1h}(s) \\ G_{21}(s) & G_{2h}(s) \\ G_{31}(s) & G_{3h}(s) \end{bmatrix} = (\mathbf{M}s^2 + \mathbf{B}s + \mathbf{K})^{-1} \quad (8)$$

Consequently, haptic device's dynamic characteristic is described by six transfer functions  $G_{11}(s)$ ,  $G_{1h}(s)$ ,  $G_{21}(s)$ ,  $G_{2h}(s)$ ,  $G_{31}(s)$ ,  $G_{3h}(s)$ . These functions have the same denominator. The transfer function  $G_{11}(s)$  can be rewritten as following:

$$G_{11}(s) = G_r(s) \cdot G_{f1}(s) \cdot G_{f2}(s) \quad (9)$$

$$G_r(s) = \frac{1}{m \cdot s^2 + b \cdot s}$$

$$G_{f1}(s) = \frac{w_{r1}^2 \cdot (s^2 + c_{a1} \cdot s + w_{a1}^2)}{w_{a1}^2 \cdot (s^2 + c_{r1} \cdot s + w_{r1}^2)}$$

$$G_{f2}(s) = \frac{w_{r2}^2 \cdot (s^2 + c_{a2} \cdot s + w_{a2}^2)}{w_{a2}^2 \cdot (s^2 + c_{r2} \cdot s + w_{r2}^2)}$$

where  $m$  and  $c$  are the total mass and the total viscous friction parameters of the device,  $w_{ri}$  and  $c_{ri}$  ( $i = 1, 2$ )

are the parameters of the  $i^{\text{th}}$  resonant mode,  $w_{ai}$  and  $c_{ai}$  are the parameters of the  $i^{\text{th}}$  antiresonant mode.

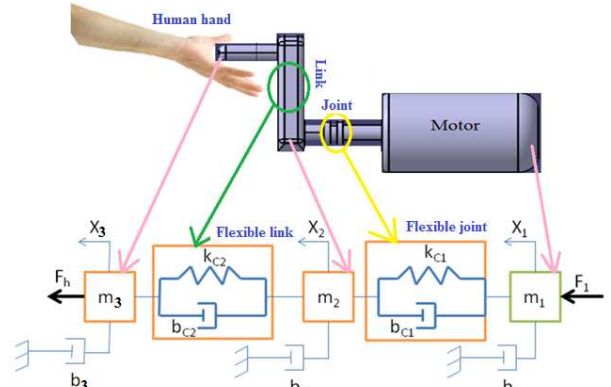


Figure 2: Haptic device model with two vibration modes

The resonant and anti-resonant frequencies are indexed by  $r$  and  $a$ , respectively.  $G_r(s)$ ,  $G_{f1}(s)$  and  $G_{f2}(s)$  are the transfer functions of the rigid mode, the first vibration mode and the second vibration mode of the haptic device, respectively. The physical parameters of the PHANTOM haptic device are given in Table 1.

Table 1 (Gil and al. 2010): Physical parameters of the PHANTOM

Parameter	Variable	Value
First vibration mode		
Inertia	$m$	1.168 gm <sup>2</sup>
Physical damping	$b$	0.0054 Nms/rad
Anti-resonant frequency	$w_{a1}$	417.612 rad/s
Damping coefficient	$c_{a1}$	80 Nms/rad
Resonant frequency	$w_{r1}$	479.166 rad/s
Damping coefficient	$c_{r1}$	83 Nms/rad
Second vibration mode		
Anti-resonant frequency	$w_{a2}$	546.626 rad/s
Damping coefficient	$c_{a2}$	90 Nms/rad
Resonant frequency	$w_{r2}$	1159.31 rad/s
Damping coefficient	$c_{r2}$	352 Nms/rad

### 3. METHODOLOGY

In order to study the stability of haptic interface, a dynamic model including different parts is established. The more critical case for haptic interface stability occurs when the manipulated object is in contact with a virtual wall. Impedance-based virtual environment for constrained motion is a coupling system including linear spring with virtual stiffness ( $K$ ) and a virtual damping coefficient ( $B$ ). The actuator position  $X_1$  is measured by an encoder. The resulting force  $F_1$  is calculated from this impedance model. It is assumed that some nonlinear phenomena (like sensor resolution, actuator saturations, etc.) are negligible. In particular, dry friction and sensor quantization can be ignored (Gil

and al. 2007). The sampling and the time delay due to the computer part (controller, virtual environment computation, and communication) are included in the haptic interface model. With the sampling process and the zero-order holder (ZOH), the overall model is a hybrid one with both continuous and discrete form, cf. Fig.3.

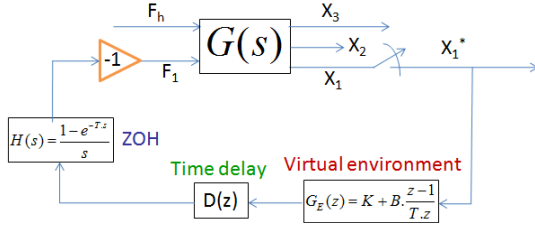


Figure 3: Dynamic model of haptic interface

From (2), the output position  $X_1$  can be written:

$$X_1(s) = G_{11}(s).F_1(s) + G_{1h}(s).F_h(s) \quad (10)$$

Combining to the dynamic model in Fig.3, the discrete form of the sampled position  $X_1^*(z)$  becomes:

$$X_1^*(z) = \frac{Z[G_{1h}(s).F_h(s)]}{1 + D(z).G_E(z).Z[G_{11}(s).H(s)]} \quad (11)$$

where  $Z[\cdot]$  denotes the Z-transform operation of a transfer function within brackets, and  $*$  designed a discrete-time signal. The virtual interface  $G_E(z)$ , the ZOH  $H(s)$  and the time delay  $D(z)$  are formulated as:

$$G_E(z) = K + B \cdot \frac{z-1}{T \cdot z}, \quad H(s) = \frac{1 - e^{-Ts}}{s}, \quad D(z) = z^{-d} \quad (12)$$

Notice that  $T$  is the sampling period and  $d$  is the time delay ratio ( $d = T_d/T$ , with  $T_d$  the total time delay). The haptic interface stability depends on the following characteristic equation:

$$1 + D(z).G_E(z).Z[G_{11}(s).H(s)] = 0 \quad (13)$$

Equation (13) can be rewritten as following:

$$1 + K \cdot \frac{D(z).Z[G_{11}(s).H(s)]}{1 + B \cdot \frac{z-1}{T \cdot z} \cdot D(z).Z[G_{11}(s).H(s)]} = 0 \quad (14)$$

Therefore, the stability boundary obtained by calculating the gain margin  $K_{critical}$  of the transfer function is defined by (Gil and al. 2007):

$$K_{critical} = Gm \left\{ \frac{D(z).Z[G_{11}(s).H(s)]}{1 + B \cdot \frac{z-1}{T \cdot z} \cdot D(z).Z[G_{11}(s).H(s)]} \right\} \quad (15)$$

where  $Gm\{\cdot\}$  represents the gain margin of the transfer function within brackets. Matlab<sup>®</sup> is used to compute the gain margin. This method is very useful to reconstruct the stability boundaries of haptic interfaces even if their transfer functions are very complex.

In the following parts, the gain margin method is used to find the stability boundaries for different values of the time delay and the anti-resonant frequency. The presented results are based on the physical parameters of the PHANTOM<sup>®</sup> (cf. Table 1).

#### 4. TIME DELAY INFLUENCE

Stability boundaries of the haptic interface model that includes two vibration modes can be found for different time-delay values by calculating (15) over a range of virtual damping values. The results for some time delay ratio values ( $d=0, 1, 2, 4, 8$ ) are shown in fig.4, with a sampling period equals to  $T = 1$  ms.

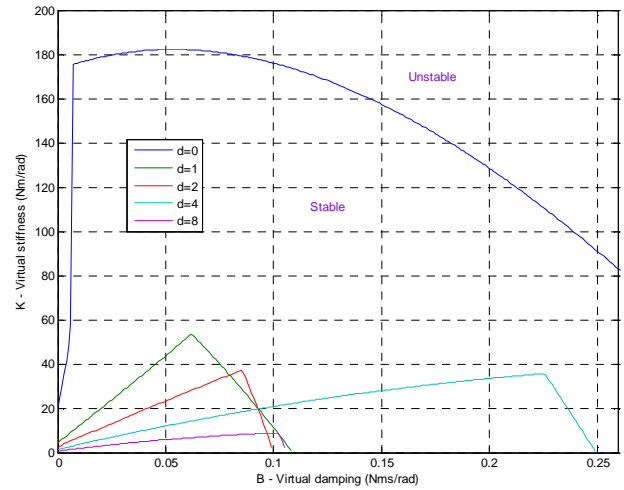


Figure 4: Stability boundaries of haptic interface model with two vibration modes for different time delay values

Let us denote  $K_{max}(B,d)$  the stability boundary that is the maximal value of  $K$  for which the system is stable for a given virtual damping coefficient  $B$  and a given time delay  $d$ . As it can be intuitively guessed, the maximal value  $K^*(d) = \max_B K_{max}(B,d)$  is a decreasing function of the time-delay value. This fact can be explained by the reduction of the phase crossover frequency (frequency at which the phase is  $-180^\circ$ ) in the Bode diagram of  $Z[G_{11}(s).H(s)].D(z)$ , cf. Fig.5. However, the stability region doesn't always decrease for rising time delay value. It is interesting to find that the stability region with a time delay of 4 ms is larger along the  $B$  axis than the stability regions with 2ms and 8ms. This behavior is explained by introducing the notion of *critical frequency*, denoted  $\omega_{cri}$ , which is defined as the maximal value of the phase crossover frequency. Obviously, the higher the critical frequency is, the larger the stability region is, cf. Fig.4 & Fig.6. These results are completely consistent with the experimental results shown by Gil and al. 2010, where

the critical frequency values of the PHANTOM were experimentally obtained by using the relay method.

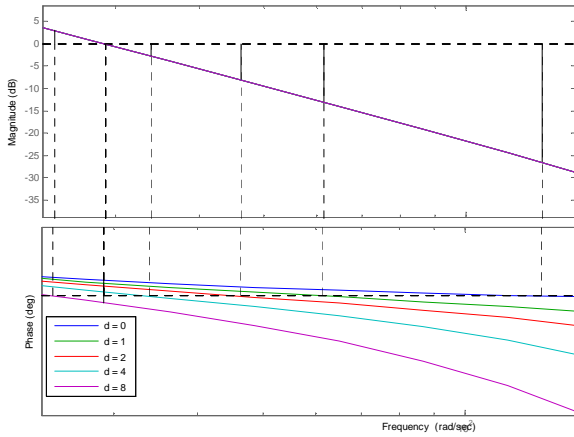


Figure 5: Bode diagram of  $Z[G_{11}(s).H(s)].D(z)$  for different time delay values

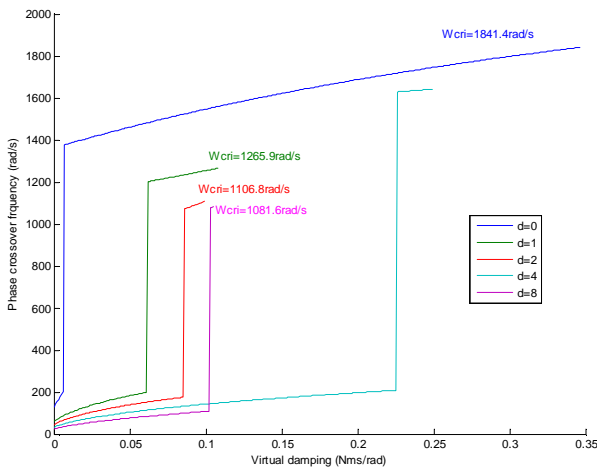


Figure 6: Phase crossover frequencies for different time delay values

## 5. ANTI-RESONANT FREQUENCY EFFECT

The linear model parameters of the PHANTOM haptic device including the two most significant vibration modes were given in the Table 1. The theoretical Bode diagram of this device is shown in fig.7.

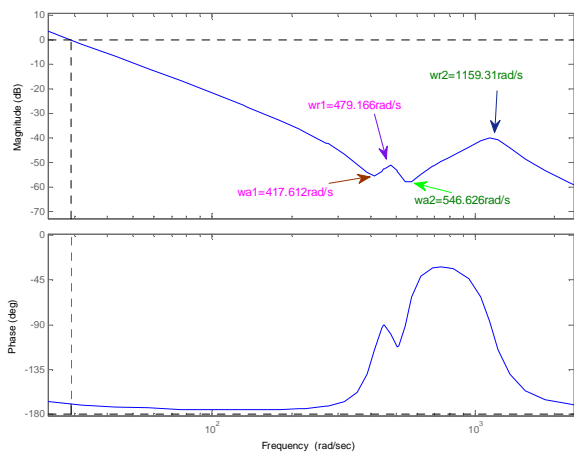


Figure 7: Theoretical Bode diagram of the PHANTOM

In the next sections, the anti-resonant frequency effects of each vibration mode are examined. Obviously the other physical parameters are considered to be constant.

### 5.1. Effect of the first vibration mode

In this part, the anti-resonant frequency effect of the first vibration mode on the haptic interface stability is examined. This frequency has to satisfy the condition (16), which allows assuring the distinction of two vibration modes as seen in fig.7. The others parameters are given in Table 1.

$$0 < w_{a1} < w_{r1} = 479.166 \text{ rad/s} \quad (16)$$

The figure 8 shows the stability boundaries of the haptic interface with the time delay ratio  $d = 1$  ( $T_d=T=1\text{ms}$ ) for some of different anti-resonant frequency values of the first vibration mode. The stability region shape changes when the anti-resonant frequency rises in the range of the condition (16). From the Bode diagram of the transfer function  $Z[G_{11}(s).H(s)].z^{-1}$ , as seen in fig.9, it is obvious that the phase crossover frequency changes from the right side to the left side of the first vibration mode.

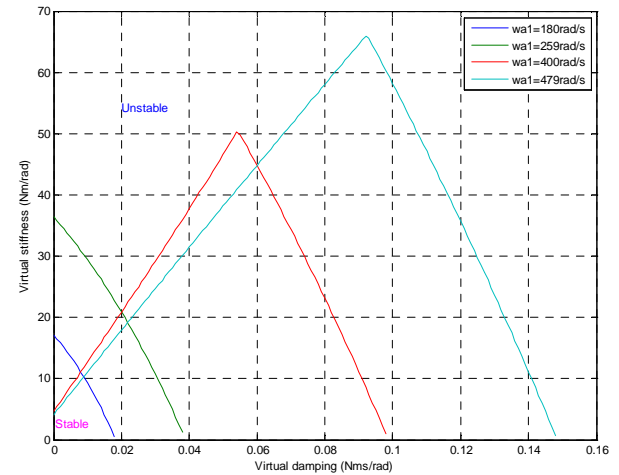


Figure 8: Stability boundaries for different values of  $w_{a1}$

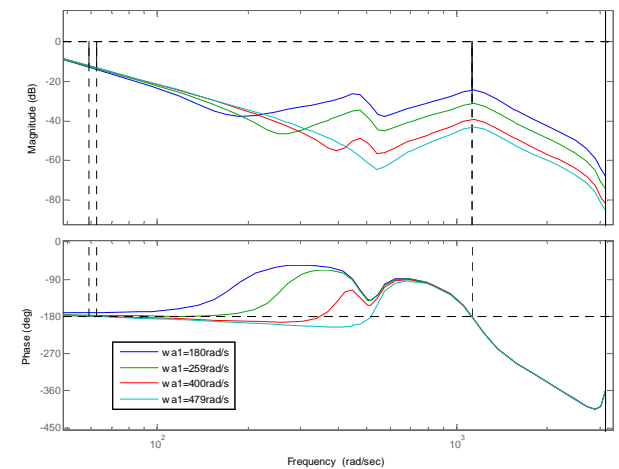


Figure 9: Bode diagram of  $Z[G_{11}(s).H(s)].z^{-1}$  for different values of  $w_{a1}$

These studies shown out the existence of a transition frequency at which there is a qualitative modification of the phase crossover frequency in the Bode diagram, and so that, it changes the stability region shape. As seen in Figs. 10 and 11, this transition frequency, denoted  $w_{at1}$ , is in the range of  $264\text{rad/s} < w_{at1} < 265\text{rad/s}$ . For  $w_{a1} \leq 264\text{rad/s}$ , the stability region increases when the anti-resonant frequency rises in this range; the phase crossover frequency is located on the right side of the first vibration mode and depends very slightly on  $w_{a1}$ . For  $265\text{rad/s} \leq w_{at1} < 479.166\text{rad/s}$ , the phase crossover frequency jumps to the left side of the first vibration mode; the stability region has a reverse V-shape including two parts: the part 1 corresponding with small values of  $B$ , the stability region decreases along the  $K$ -axis, the part 2 corresponding with higher values of  $B$ , the stability region increases along the  $B$ -axis when the anti-resonant frequency rises in its range.

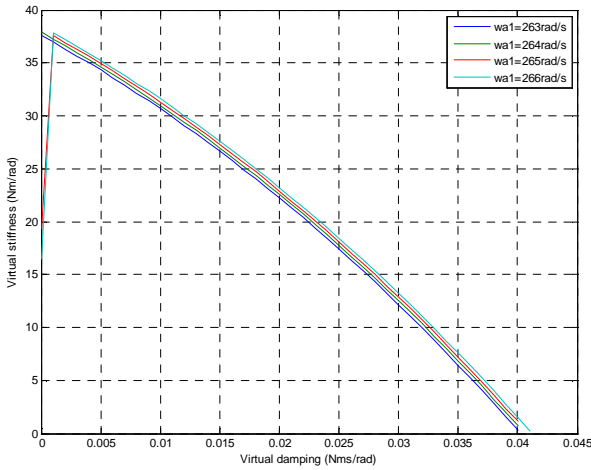


Figure 10: Stability boundaries for different values of  $w_{a1}$  around the transition frequency  $w_{at1}$ .

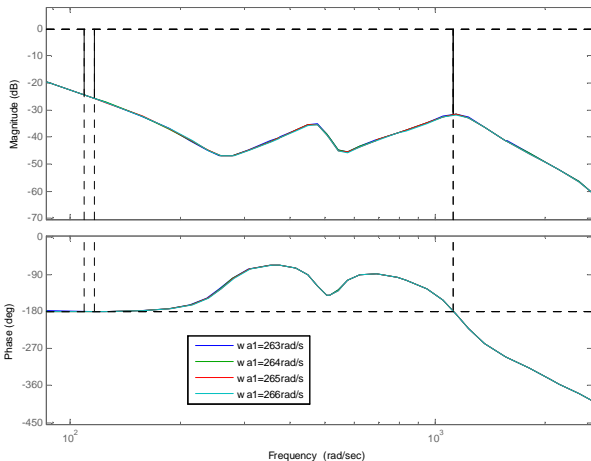


Figure 11: Bode diagram of  $Z[G_{11}(s).H(s)].z^{-1}$  for different values of  $w_{a1}$  around the transition frequency  $w_{at1}$ .

## 5.2. Second vibration mode effect

The anti-resonant frequency effect of the second vibration mode on the haptic interface stability is

studied with the condition (17) in order to assure the distinction of two vibration modes as seen in Fig. 7. The others parameters can be found in Table 1.

$$w_{r1} = 479.166\text{rad/s} < w_{a2} < w_{r2} = 1159.31\text{rad/s} \quad (17)$$

As shown in Figs. 12-13, although the phase crossover frequencies in the Bode diagram of the transfer function  $Z[G_{11}(s).H(s)].z^{-1}$  are always located on the left side of two vibration modes, the stability regions of the haptic interface with the time delay ratio  $d=1$  ( $T_d=T=1\text{ms}$ ) for some of anti-resonant frequency values of the second vibration mode are very different shapes.

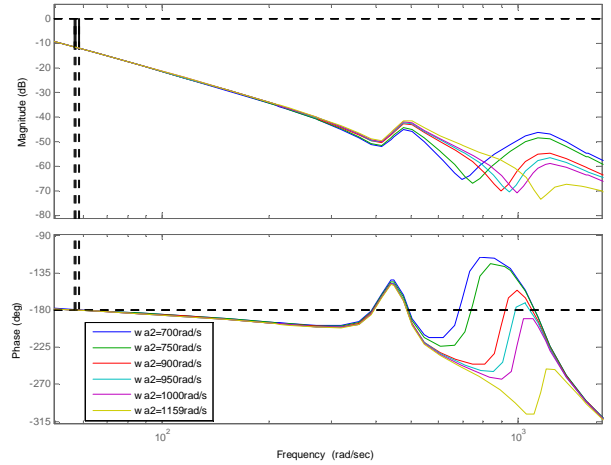


Figure 12: Bode diagram of  $Z[G_{11}(s).H(s)].z^{-1}$  for different values of  $w_{a2}$

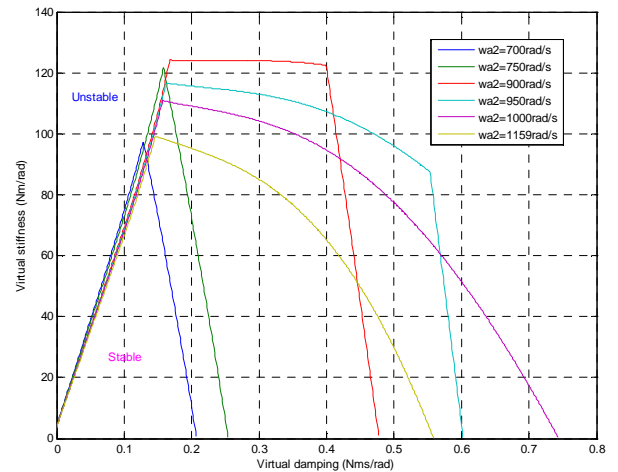


Figure 13: Stability boundaries for different values of  $w_{a2}$

Obviously, for small values of  $B$ , the stability region is most linear and decreases gradually along the  $K$ -axis with the increasing values of  $w_{a2}$  (cf. Fig. 14). It is noteworthy that this linear region can be explained by the Bode diagram of the transfer function  $Z[G_{11}(s).H(s)].z^{-1}$ . The larger linear stability region corresponds with the bigger value of the phase crossover frequency (cf. Fig. 15).

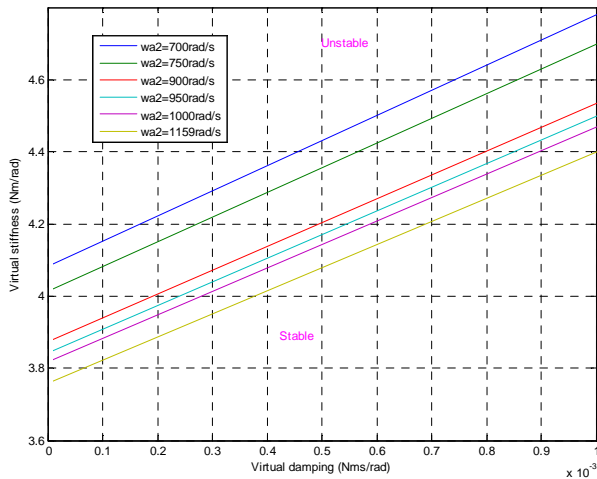


Figure 14: Partial view of the stability regions for different values of  $w_{a2}$

## 6. CONCLUSIONS

This paper has introduced an overview on the stability analysis with respect to the time delay and the two first vibration modes of the haptic interface model. The impedance model has been used to compute the force feedback including a virtual stiffness and a virtual damping. The stability boundaries of both virtual parameters have been derived from a sampled-data model with the gain margin method. The stability analysis is based on the linear model with two vibration

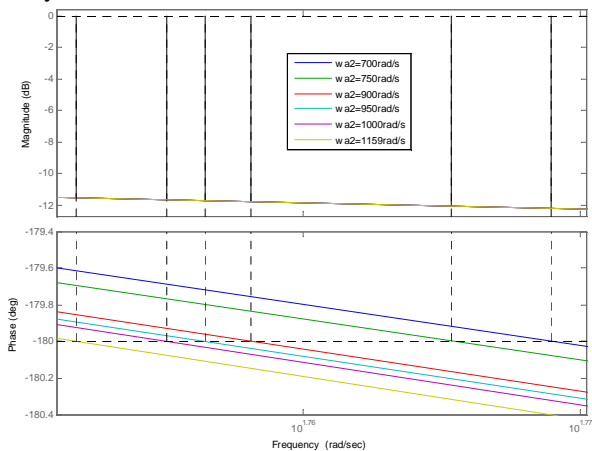


Figure 15: Partial view of the Bode diagram of  $Z[G_{11}(s).H(s)].z^{-1}$  for different values of  $w_{a2}$  (the left side of two vibration modes)

modes of a haptic device and the effects on stability of each mode have been detailed. The presented results allow us to conclude that the haptic device's vibration modes have an intricate effect on the interface stability. The analysis of the anti-resonant frequency effect leads to explanations about qualitative modification of stability boundaries. These results may provide some basic engineering guidelines in choosing design specifications of a haptic system.

Haptic devices have stability limitations that can be overcome by incorporating feedback controllers or

signals shapers (Kuchenbecker 2006). While the uncertainties on model parameters is a key issue for flexible mechanism (Dieulot and Colas 2009), robust control design can play an important role in haptic interface design.

## ACKNOWLEDGMENTS

This work was supported in part by the International Campus on Safety and Intermodality in Transportation, the European Community (through the FEDER European Funds for Regional Development), the Délégation Régionale à la Recherche et à la Technologie, the Ministère de l'Enseignement supérieur et de la Recherche, the région Nord Pas-de-Calais and the Centre National de la Recherche Scientifique (CNRS). The authors gratefully acknowledge the support of these institutions.

## REFERENCES

- Adams, R.J., Hannaford, B., 1998. A Two-Port Framework for the Design of Unconditionally Stable Haptic Interfaces. *Proceedings of the IEEE/RSJ International Conference on Intelligent Robots and Systems*, Victoria, BC.
- Adams, R.J., Moreyra, M.R., Hannaford, B., 1998. Stability and Performance of Haptic Displays: Theory and Experiments. *Proceedings of the ASME International Mechanical Engineering Congress and Exhibition*, Anaheim, CA.
- Adams, R.J., Hannaford, B., 1999. Stable Haptic Interaction with Virtual Environments. *IEEE Trans. on Robotics and Automation*, 15(3), 465–474.
- Adams, R.J., Hannaford, B., 2002. Control Law Design for Haptic Interfaces to Virtual Reality. *IEEE Trans. on Control Systems Technology*, 10(1), 3–13.
- Colgate, J.E, Brown, J.M., 1994. Factors affecting the Z-Width of a Haptic Display. *Proceedings of the IEEE International Conference on Robotics and Automation*, May, San Diego, CA.
- Colgate, J.E., Schenkel, G., 1997. Passivity of a class of sampled-data systems: Application to haptic interfaces. *Journal of Robotic Systems*, 14(1), 37–47.
- Diolaiti, N., Niemeyer, G., Barbagli, F., Salisbury, J. K., 2006. Stability of haptic rendering: Discretization, quantization, time-delay and Coulomb effects. *IEEE Trans. on Robotics*, 22(2), 256–268.
- Díaz, I., Gil, J.J., 2008. Influence of Internal Vibration Modes on the Stability of Haptic Rendering. *Proceedings of the IEEE International Conference on Robotics and Automation*, May, Pasadena, CA.
- Díaz, I., Gil, J.J., 2010. Influence of Vibration Modes and Human Operator on the Stability of Haptic Rendering. *IEEE Trans. on Robotics*, 26(1), 160–165.
- Dieulot J.-Y., Colas F., 2009. Robust PID control of a linear mechanical axis: A case study. *Mechatronics* 19(2), 269-273

- Gil, J.J., Avello, A., Rubio, Á., Flórez, J., 2004. Stability analysis of a 1 DOF haptic interface using the Routh–Hurwitz criterion. *IEEE Trans. on Control Systems Technology*, 12(4), 538–588.
- Gil, J.J., Sanchez, E., Hulin, T., Preusche, C., Hirzinger, G., 2007. Stability boundary for haptic rendering: Influence of damping and delay. *Proceedings of the IEEE International Conference on Robotics and Automation*, Roma (Italy).
- Gil, J.J., Puerto, M.J., Díaz, I., Sánchez, E., 2010. On the Z-Width Limitation due to the Vibration Modes of Haptic Interfaces. *IEEE Trans. on Robotics*, 26(1), 160-165.
- Hulin, T., Preusche, C., Hirzinger, G., 2006. Stability boundary for haptic rendering: Influence of physical damping. *Proceedings of the IEEE/RSJ International Conference on Intelligent Robots and Systems*, October 9-15, Beijing (China).
- Hulin, T., Preusche, C., Hirzinger, G., 2008. Stability boundary for haptic rendering: Influence of human operator. *Proceedings of the IEEE/RSJ International Conference on Intelligent Robots and Systems*, September 22-26.
- Kuchenbecker K. J., 2006. Characterizing and controlling the high-frequency dynamics of haptic interfaces, Thesis (PhD). Stanford University.